A&A 580, A16 (2015)
DOI: 10.1051/0004-6361/201525618

Astronomy & Astrophysics

Case studies of multi-day ^{3}He-rich solar energetic particle periods

Nai-hwa Chen[1], Radoslav Bučík[1], Davina E. Innes[1], and Glenn M. Mason[2]

[1] Max-Planck-Institut für Sonnensystemforschung, 37077 Göttingen, Germany
e-mail: chenm@mps.mpg.de
[2] Applied Physics Laboratory, Johns Hopkins University, Laurel, MD 27023, USA

Received 6 January 2015 / Accepted 13 May 2015

ABSTRACT

Context. Impulsive solar energetic particle events in the inner heliosphere show the long-lasting enrichment of ^{3}He.
Aims. We study the source regions of long-lasting ^{3}He-rich solar energetic particle (SEP) events
Methods. We located the responsible open magnetic field regions, we combined potential field source surface extrapolations with the Parker spiral, and compared the magnetic field of the identified source regions with in situ magnetic fields. The candidate open field regions are active region plages. The activity was examined by using extreme ultraviolet images from the Solar Dynamics Observatory (SDO) and STEREO together with radio observations from STEREO and WIND.
Results. Multi-day periods of ^{3}He-rich SEP events are associated with ion production in single active region. Small flares or coronal jets are their responsible solar sources. We also find that the ^{3}He enrichment may depend on the occurrence rate of coronal jets.

Key words. Sun: corona – Sun: UV radiation – Sun: radio radiation – solar-terrestrial relations

1. Introduction

Measurements in the past few decades show that solar energetic particles (SEPs) are accelerated in the shocks of coronal mass ejections (CMEs) and during flares (for a detailed review see in Reames 1999, and the references therein). The former are generally believed to be responsible for gradual SEP events, and the latter are the likely source of impulsive SEP events (Cliver et al. 1983; Cane et al. 1986, 1988; Kahler et al. 1984). It is known that the impulsive SEP events have a higher ^{3}He/^{4}He isotopic ratio and heavier ion enhancement than in the average corona (Hsieh & Simpson 1970; Mason et al. 1986). These ions are understood to be accelerated and released above the region where hard X-rays and microwaves are emitted, as inferred from radio observations (Klein & Posner 2005). The high mean ionic charge state of ions found in impulsive SEP events suggests that the temperature of the source region could reach 10^7 K (Klecker et al. 1984; Luhn et al. 1987) in turn suggesting the acceleration site at an altitude less than 0.2 Rs (Klecker et al. 2007). Resonant wave-particle interactions in the flare site are thought to be the acceleration mechanisms for ^{3}He-rich SEP events (Fisk 1978; Temerin & Roth 1992). There have been several cases reported in which the ^{3}He flux persisted above the background for a few days, suggesting a steady and continuous acceleration of ^{3}He ions in their source sites (Mason 2007; Kocharov et al. 2008).

In the Solar and Heliospheric Observatory (SOHO) era, it was shown that small brightenings or jets at or near active region (ARs) on the western hemisphere were the source regions of ^{3}He-rich SEP events as inferred from extreme ultraviolet (EUV), white light, and radio observations (Wang et al. 2006; Pick et al. 2006; Nitta et al. 2006). In their studies, recurrent coronal jets were seen from the connected ARs for a period of 1−2 days around the time of the ^{3}He-rich SEP event. Coronal jets are often seen when flux emerges into open field regions, which leads to reconnection between the emerging flux and open fields (Yokoyama & Shibata 1996; Moreno-Insertis et al. 2008; Archontis et al. 2010). Jets are also commonly observed on the edge of sunspots (Canfield et al. 1996; Nitta & De Rosa 2008; Innes et al. 2011) and in AR plages (Wang et al. 2006; Pick et al. 2006). The close temporal correlation between ^{3}He-rich SEP events, jets, and kilometric type III radio bursts suggests that the energetic particles are accelerated via magnetic reconnection (Lin 1985; Reames et al. 1985; Reames & Stone 1986; Kundu et al. 1995; Krucker et al. 2011; Klassen et al. 2011).

In this paper, we examine the source regions of SEPs whose ^{3}He-rich period lasts for 4−5 days. The investigated ^{3}He-rich SEP events were observed by Advanced Composition Explorer (ACE). In Sect. 2, we investigate the source regions identified with the help of coronal magnetic field extrapolations, and the associated activity on the solar disk seen in solar EUV images of the Atmospheric Imaging Assembly (AIA) on board the Solar Dynamics Observatory (SDO) and the Extreme UltraViolet Imager (EUVI)/STEREO-A. The results are summarized and discussed in Sect. 3.

2. Observation and data analysis

2.1. ^{3}He-rich SEP events

We investigate the solar sources of two long-lasting ^{3}He-rich periods on 2010 November 14−18 and 2012 November 18−21 (Fig. 1c). Each consists of two individual events. The helium ions were detected by the Ultra Low Energy Isotope Spectrometer (ULEIS; Mason et al. 1998) on ACE at the L1 Lagrangian point. We first estimate the release time window of the ^{3}He-rich SEP events based on the ion energy of 0.23−0.32 MeV nucleon^{-1}. Under the assumption that these particles travel scatter-free along the spiral path length of 1.2 AU, it is about 5−8 h prior to event start time for events showing energy dispersion in the inverse velocity-time spectrograms. The

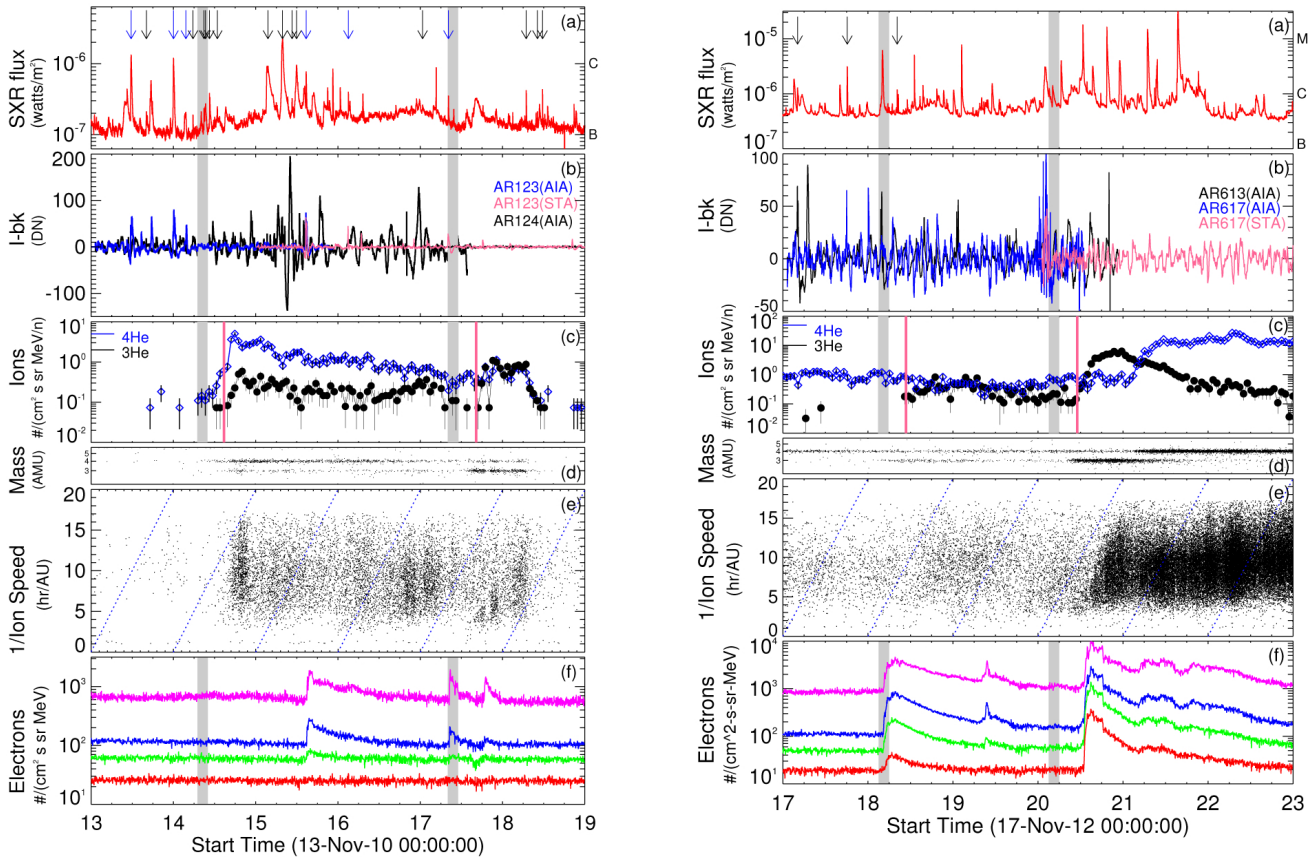

Fig. 1. Summary of multi-day ^{3}He periods and related solar activity. *Left*: Period 1, *right*: Period 2 **a)** GOES SXR flare flux in the energy band of 1−8 Å. Arrows at the top point to the SXR flares in the candidate ARs and flares in other ARs are not marked. **b)** The EUV 193 Å excess intensity, the average AR flux (see Sect. 2.1) observed by AIA/SDO and STA in AR11124 (black); 11123 (blue, purple) in period 1 and AR11613 (black); and 11617 (blue, purple) in period 2. The intensity extension of AR11123 and 11617, which are integrated in EUVI/STA, is shown in purple for two periods. ARs are labeled with the last three digits of their names e.g., AR11124 is labeled as 124. **c)** 0.23−0.32 MeV/n 1 h averaged ^{3}He (black) and ^{4}He (blue) intensity observed by ULEIS/ACE. The purple lines show the approximate start time of each event at 1 AU, shown in Table 1. **d)** Helium mass spectrogram in energy range 0.4−10 MeV/n. **e)** Inverted ion velocity time spectrogram in mass range 10−70 AMU. **f)** The 5 min averaged electron intensity at EPAM/ACE in four energy bands: 0.038−0.053 MeV(purple), 0.053−0.103 MeV(blue), 0.103−0.175 MeV (green), and 0.175−0.315 MeV (red). The gray regions mark the time window for the ^{3}He ions release time from the Sun (see Sect. 2.1).

Table 1. ^{3}He-rich SEP events in this study.

Event	Start time (UT)	End time (UT)	^{3}He/^{4}He (ACE)
1	2010-Nov.-14 15:00	2010-Nov.-17 09:00	0.2
	2010-Nov.-17 16:00	2010-Nov.-18 10:00	2.8
2	2012-Nov.-18 11:00	2012-Nov.-20 06:00	1.0
	2012-Nov.-20 11:00	2012-Nov.-21 04:00	6.7

Notes. The ion event starting time is inferred from ^{3}He intensity time profiles in energy of 0.23−0.32 MeV/n and the ratios are from energy of 0.32−0.45 MeV/n.

release time for dispersionless events is difficult to estimate because the spacecraft connects to field lines previously populated with SEPs. Table 1 contains the approximate start/end times of the ion events at 1 AU and events summed the ^{3}He/^{4}He ratios (Bucik et al. 2013). We list the flares that occurred close to the release time windows and the related type III and type VI bursts in Table 2. These are based on the Space Weather Prediction Center (SWPC) daily solar event report. Type VI are a series of type III bursts over a period of 10 min or more. The activity at the Sun during the ^{3}He-rich SEP periods is summarized as soft X-ray and EUV light curves in Fig. 1. Here we show in panel a GOES soft X-ray (SXR) flux (1−8 Å), and in panel b the spatially-averaged EUV 193 Å flux of associated source regions, discussed further in Sect. 2.3. The EUV flux is integrated over the dashed boxes (see Fig. 4) in the AIA observations with the 30-min average background subtracted. The STA observations are also added when the ARs cross the limb. The background is possibly influenced by the duration and the occurrence rate of flares. Negative intensity is sometimes caused by a large background, which is due to the overlap of two close flares. Also shown are panel c ^{3}He and ^{4}He ions flux observed by ULEIS/ACE, panel d helium mass spectrogram, panel e inverted ion velocity time spectrogram, and panel f 5-min averaged electron intensity in EPAM/ACE in the energy channels between 38−315 keV.

Table 2. GOES SXR Flares and type III/VI bursts around the estimated time windows.

Period	Date	Flare start/peak time (UT)	GOES class	Active region	Type III/VI bursts time
1	2010-Nov.-13	23:50/00:01	C1.0	11123	23:40(−00:02) (type VI)
	2010-Nov.-14	03:08/03:38	B2.0	11123	
		08:52/08:55	B2.2	11124	
		09:08/09:22	B2.6	11124	
	2010-Nov.-17	08:07/08:12	B3.4	11123	08:08(−08:10)
2	2012-Nov.-18				00:06−00:09
					03:27−03:30
				11615	03:46(−04:13) (type VI)
		03:55/ 04:07	C5.7	11615	04:00(−04:07)
					07:28(−07:29)
	2012-Nov.-19				23:40
	2012-Nov.-20				00:18
					01:29
		01:37/ 02:07	C3.0	11618	02:10
				11617	02:32(−02:39) (type VI)
					03:09
					03:29
		04:04/ 04:10	C1.3	11618	

Notes. The bold AR11617 in 2012-Nov.-20 shows the corrected source of the type III burst that we identified (see Sect. 2.1.2).

2.1.1. 2010 November 14−18

Period 1, shown in the left panels of Fig. 1, consists of two individual ^{3}He flux increases, one starting on Nov. 14 and the other on Nov. 17. The first increase on Nov. 14 showed an ^{3}He/^{4}He ratio of ∼0.20 (0.32−0.45 MeV nucleon^{-1}) but no accompanying electron event was observed. The possible associated SXR flares in the estimated time window were two B-class flares from AR11124 with start time at 08:52 and 09:08 UT. We note that these were not associated with type III emission. The November 14 event shows a dispersionless onset, where ions of different speeds enhance simultaneously. It occurs when the spacecraft encounters a magnetic flux tube already filled with energetic ions. The ion release time most likely occurred before the indicated time window. The second increase on November 17 had a higher ^{3}He/^{4}He ratio of ∼2.75. It was associated with a B3.4 SXR flare in AR11123, which peaked at 08:12 UT. It was accompanied by an impulsive electron event and the ion velocity dispersion was clearly evident (indicated by the typical triangular pattern). We also searched for type III radio bursts in WIND/WAVES data that occur close to the release time window, shown in Fig. 2. The red bars mark the estimated release time windows. An expanded view of panel a around the time of the red bars is given in panels b and c below. Since there was no electron event associated with the first ^{3}He increase, it is not surprising that there was no type III burst found in our time window. Earlier VI/III bursts were observed at 23:40 UT, Nov. 13, and 03:08 UT, Nov. 14. These two bursts were accompanied by C1.0 and B2.0 flares, respectively, in AR11123 (see Table 2). In the second ^{3}He increase, a type III burst with an onset at 08:10 UT was clearly observed and was accompanied by a B3.4 flare in AR11123.

2.1.2. 2012 November 18−21

The corresponding plots for period 2 are shown in the right panels of Fig. 1. The energetic ^{3}He flux increase began on Nov. 18 with another enhancement observed on Nov. 20 (panel c). The first increase, with ^{3}He/^{4}He ratio of ∼1.0, was accompanied by a C5.7 SXR flare from AR11615 and an electron event with a longer duration. The ^{3}He-rich event has no clear velocity dispersion. The radio observations in the right panel b of Fig. 2 showed a type III/VI burst associated with the C5.7 flare, starting at 03:46 UT in the release time window. In addition, the 0.4−10 MeV/n ^{3}He was already present at the flare start time (see the mass spectrogram, panel d). Therefore this event probably originated from an earlier release, but the contribution of ^{3}He later during the event cannot be ruled out. There was a type III burst with onset at 00:06 UT which is under our consideration for the possible earlier release. This has no associated source region in the SWPC report. The second increase showed a ^{3}He/^{4}He ratio of 6.7, but no corresponding electron event was observed. The prominent electron event later was related to the M1.7 SXR flare with the onset time at 12:36 UT. The ^{3}He-rich event velocity dispersion was clearly evident. The two C-class SXR flares that occurred close to the time window (Table 2) were from AR11618, located in the eastern hemisphere. Five type III/VI bursts were observed between 01:00 and 04:00 UT, Nov. 20. Among them, two bursts (marked by arrows of the right panel c in Fig. 2) with onset at 01:29 and 02:32 were quiet strong, showing a deep drift below 0.1 MHz. The source AR for the 01:29 UT burst was not reported and for the 02:32 UT the source in the SWPC list, AR11618, was likely erroneous. AR11618 (E27) was located near the west limb (W98) in the STEREO-B (STB) view and thus not far from the spacecraft magnetic connection point, but no type III burst was seen by the WAVES/STB radio instrument. However, STA observed the same 01:29, 02:32 type III bursts even though the purported source AR11618 was at the back side of the Sun (E155) from the STA view. This makes it very unlikely that AR11618 was the source of these two type III bursts. On the other hand, AR11617 shows a clear EUV brightening at the same time as type III burst at 02:32 UT (Sect. 2.3). Additionally, a weak narrow coronal mass ejections (CME), observed by LASCO (Large Angle and Spectrometric Coronagraph)/SOHO, lifted off from the west limb at the time between 2:30 and 4:00 UT after the brightening seen on AR11617. The lack of the associated electron event might be due to the observational effect. The electron intensity level is slightly higher due to the previous two electron events which might mask the related small event. We note

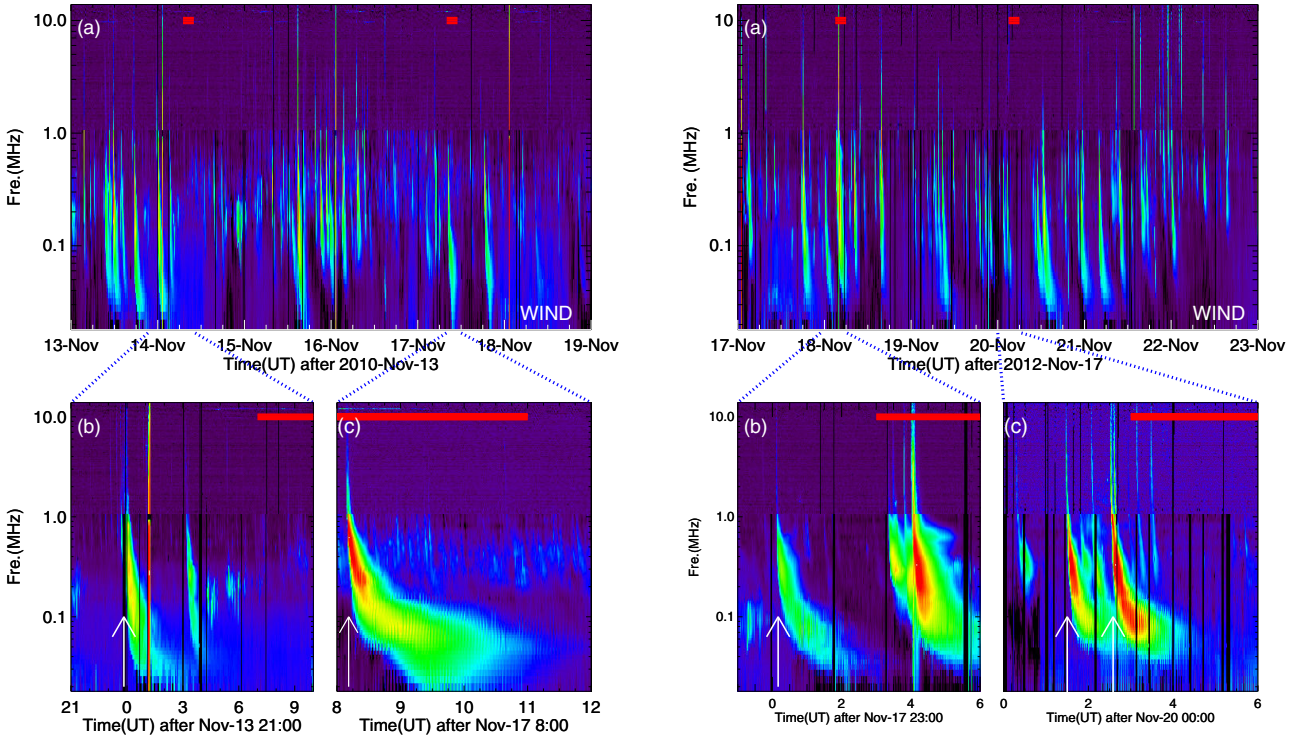

Fig. 2. Kilometric radio observations. *Left*: period 1; *right*: period 2. Panel **a)**: kilometric radio observations on WIND/WAVE in two events. The red bars mark the ion release time windows shown as the dashed regions in Fig. 1. Panels **b)** and **c)** are enlarged views of the time ranges around each event associated type III radio burst, indicated by white arrows.

that the previous studies reported only ~60% association with the electron events (e.g., Nitta et al. 2006).

For the two periods, not all the investigated ^{3}He increases are related to electron events or show velocity dispersion. Thus their origins are not clearly evident in the energetic ion temporal profiles, SXR flare, and radio observations. To further narrow down the possible source regions, we examine the magnetic field connection and EUV images in the next sections.

2.2. Magnetically connected regions

To find the source regions of the investigated ^{3}He-rich SEP events, we determine the connectivity from the Sun through the corona and interplanetary space to Earth by the method combining the potential field source surface (PFSS) model and Parker spiral. It has been used to identify the sources of ^{3}He-rich SEP events in previous investigations (Nitta et al. 2006; Wang et al. 2006). The data source used for the PFSS model here, which is available via Solar Soft PFSS package[1], is based on the SDO Helioseimic and Magnetic Imager (HMI) magnetograms. In addition, the in situ magnetic polarity is compared with the results of PFSS model in this study. We trace the field lines back from the source surface at 2.5 R_{sun} to the photosphere using the PFSS model (Schrijver & De Rosa 2003). The interplanetary magnetic field between the source surface and the spacecraft, assumed as a Parker spiral is a function of the measured solar wind speed. In Fig. 3, the open field lines are overplotted on the photospheric magnetic maps that were reconstructed at the start times (see Table 1) of the ^{3}He enrichments. The green and red lines represent the positive and negative polarities, respectively. The colorbar above the map indicates the in situ magnetic polarity during the time of ^{3}He periods with the same color index as the field line tracing (e.g. green indicates the magnetic field pointing away from the Sun). The in situ polarity is determined by the angle between the observed magnetic field and the Parker spiral model magnetic field using the measured solar wind speed on ACE. When the angle is within ±20°, of the normal Parker field direction, yellow is used.

Figures 3a and b show magnetic connections for the 2010 November 14 and 17 events, respectively. The in situ magnetic polarity suggests that on November 14, ACE was connected via negative (red) field to AR11123 or to the coronal hole located below AR11124. The PFSS extrapolations for November 17 suggests the connection to AR11124. However, at this time, AR11123 was very close to the west limb so the magnetic field was poorly measured and the PFSS extrapolation may not reflect the field as it was. We therefore require EUV data to identify the source region.

The corresponding maps for the 2012 November 18 and 20 events are shown in Figs. 3c and d. Multiple regions on the solar surface revealed the complexity during this ^{3}He-rich period. It was also seen that the in situ magnetic polarity changed several times to the negative or uncertain (yellow) polarity, but the main connection was via the positive field (green). The in situ polarity suggests its connection through the positive field to the area adjacent to AR11617 and AR11613 for both November 18 and 20.

2.3. EUV observations in the associated active regions

We use the AIA 193 Å 1 min and EUVI/STA 5 min 195 Å image observations to study the EUV variation in the candidate ARs during the investigated periods. The 193 Å channel primarily centered on Fe XII line is sensitive to the warm plasma in the vicinity of ARs at 1.6 MK and secondarily (Fe XXIV) to

[1] http://www.lmsal.com/_derosa/pfsspack

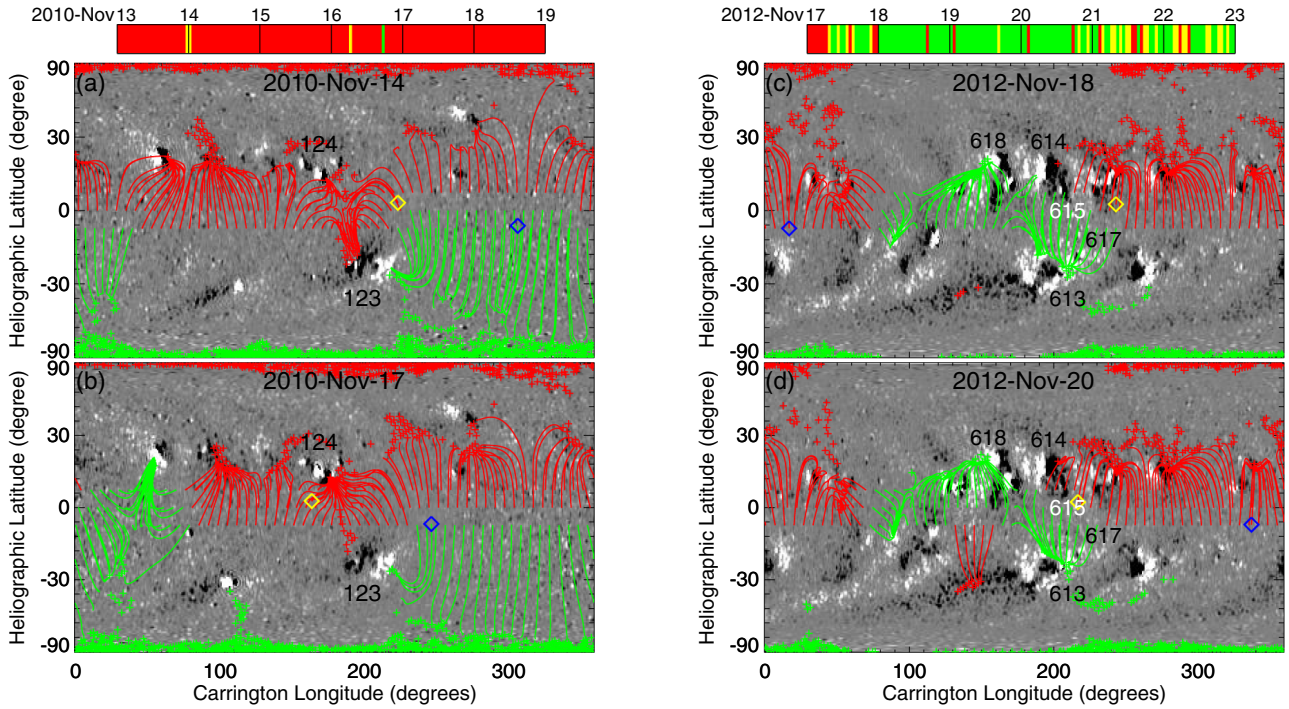

Fig. 3. The photospheric magnetic field synoptic map with coronal magnetic field lines derived from the PFSS model at the times of the ^{3}He ions flux increases. The green and red lines represent the positive and negative polarity open field lines that intersect the source surface at latitudes 0° and ±7°. Field lines that are open at the ecliptic are shown by lines and other regions of open field are denoted as crosses. The color bars above indicate the interplanetary magnetic field polarity. The yellow and blue diamonds show the footpoint of Earth and STA on the source surface, respectively. We note that the data source of the map is based on HMI magnetograms (grey scale) and the time runs from right to left in the map. ARs are labeled with the last three digits of their names e.g., AR11124 is marked at 124.

18 MK plasma. Figure 4 shows images of the candidate ARs for the two periods. The dashed boxes mark the regions of interest over which the ARs light curves are integrated. The selected boxes are centered on the regions with the conspicuous appearance of jet-like emissions or flaring in the main loops. We also show an STA observation of AR11123 when it was at the west limb in the AIA images. The bottom panels are the HMI magnetograms of each candidate.

2.3.1. 2010 November 14–18

The EUV intensity and running-difference images of the candidates AR11123 and 11124 are shown in Figs. 4a–c at the onset of associated type III radio bursts. In the background-subtracted EUV light curve of two candidate ARs (Fig. 1b, left), the EUV spikes in AR11123 were stronger than those generated by AR11124 in the early two days and then activity on AR11124 increased at the rest of time. Those EUV spikes in AR11124 were attributed to the jet-like emissions and AR11123 was in favor of flaring. For the two ion release time windows, clear EUV spikes, peaked at Nov. 14 00:01 03:38 UT and Nov. 17 08:12 UT (C1.0, B2.0, and B3.4 flares), coincided with two type III/VI bursts on November 14 (Figs. 4a, b) and the type III burst on November 17 (Fig. 4c) were observed in AR11123, but no simultaneous brightening appeared in AR11124. During the multiday event starting on Nov. 14, an EUV spike (B7.6 flare) at Nov. 15 14:38 UT with an associated electron event and a simultaneous type III burst also originated in AR11123. Throughout the whole period, small flares emanated from AR11123 and could contribute to the observed ^{3}He enrichment.

2.3.2. 2012 November 18–21

The corresponding EUV images of the two nearby candidates AR11613 and 11617, are shown in Figs. 4e–g at the onset of the associated type III radio bursts. Their intensity integrations (Fig. 1b right) showed numerous spikes produced by jets during this period. In the first enrichment, an intense EUV spike of AR11617 in EUV light curve was observed contemporarily with type III burst on November 18 00:06 UT (also seen in Fig. 4e). The second enrichment, seen on November 20, was preceded by an increase in jet activity from AR11617 (see Fig. 1b, right). Among them, two distinct jets (01:30, 02:33 UT) from AR11617 were clearly evident in the AIA images coinciding with two type III/VI bursts on November 20 (see Figs. 4f and g). These jets were clearly observed shortly after the type III burst and before the ^{3}He abundance increase. Thus, the frequent jets from AR11617 are associated with the energetic ^{3}He production in this period.

The magnetograms, at the beginning time of each release window in two periods, show where jets or flares in our candidates occurred. The jet-produced area of AR11124 originated from the west edge of a sunspot, shown in the panel d, while AR11123 was an AR plage. AR11617, where numerous jets were produced, was also an AR plage (see Fig. 4h).

The AIA/SDO observations have much higher cadence and spatial resolution than the EUV Imaging Telescope in the previous works (Wang et al. 2006; Nitta et al. 2006), which suggests the reasonable sources in the temporal investigation. The HMI magnetograms show that the activity of our candidate sources emanate from a plage region. Our observations provide evidence that the flaring/jet on a single AR is responsible for the ^{3}He abundance increase during the whole period.

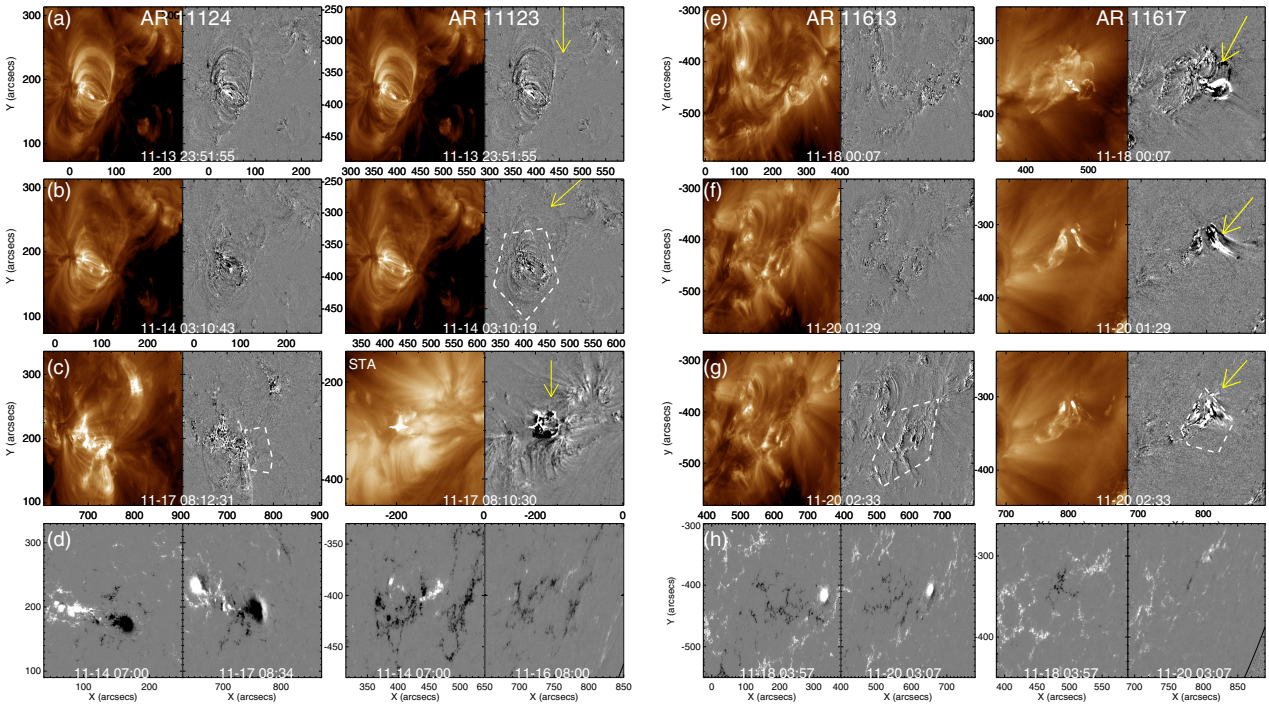

Fig. 4. AIA observations on the related source regions. **a)**–**d)** period 1-AR11123, 11124, **e)**–**h)** period 2-AR11613, 11617 The AIA 193 Å intensity/running difference images in the candidate ARs at times of type III radio bursts in two periods. The flaring/jets are indicated by the yellow arrows. Panels **d)** and **h)** are the HMI magnetograms of each candidate at the beginning time of each release window. For AR11123, nearly invisible at Nov. 17, we choose Nov. 16 instead. The dashed boxes are the integrated regions for the EUV light curves in Fig. 1b.

3. Discussion and summary

We have studied the solar origins of two long-lasting ^{3}He-rich SEP periods by analyzing high cadence coronal images. The source regions during the two periods, determined by the PFSS extrapolations of photospheric magnetic field together with EUV and radio observations, appear to be single ARs with a long steady connection to the observer. The source regions of two huge ^{3}He abundance events (^{3}He/^{4}He > 1) produce flares/jets with correlated type III/VI bursts. These impulsive SEP events show clear velocity dispersion onsets. For the two dispersionless events, the timing of type III bursts are used to determine the possible sources due to their high association with 3He-rich SEP event (Reames et al. 1985; Nitta et al. 2006).

The 2010 November 14 and 17 events were associated with AR11123 when it was at W26-W28 and near the west limb (W91), respectively. The 2012 November 18 and 20 events were associated with AR11617 when it was at W33 and W70, respectively. Previous single spacecraft observations have reported multiple events over a two-day period (Reames & Stone 1986; Wang et al. 2006; Mason et al. 2000). The coronal field extrapolations in our candidate regions revealed substantial longitudinal spread of the ecliptic field lines allowing connection for a longer period. Multiple observations with widely separated spacecraft have suggested that ARs may produce 3He-rich SEP events even for a quarter of a solar rotation (Bučík et al. 2014). It has also been suggested that multiday periods of 3He-rich SEPs may be due to confinement of the ions in the co-rotating interaction regions in the solar wind (Kocharov et al. 2008). Mason (2007) has suggested a continuous injection from the solar sources when onset was not obvious.

We have shown two multi-day periods associated with the same source where the first events show lower ^{3}He-enrichment than the second ones. In the 2012 November 18–21 period, numerous recurrent EUV jets occur in AR11617, an AR plage, for six hours (from the November 19 22:00 UT to November 20 4:00 UT) preceding the second event. Their magnitude and especially the frequency of occurrence largely increases. A type VI burst accompanied by these jets suggests the continuous accelerations and ejections of low-energy electrons from the source site for a longer time than single normal type III burst does. It might suggest that huge ^{3}He abundance in the second event is due to the continuous processes in its source. In the 2010 November 14–18 period, the responsible activity is flaring instead of the jetting. Source AR11123 has generated many small flares since its maximum phase (on November 11, see Mandrini et al. 2014) and decay during our investigated period. The sizes of two responsible flares are different by one order of magnitude. Stronger ^{3}He enrichment in later time is associated with the smaller flares (B3.4) which is consistent with previous works (Reames et al. 1988; Reames 1999).

Our observations provide evidence that the production and release of ^{3}He-rich SEPs from a single AR may be a common process. Small flares or coronal jets, noted in previous works, appear to be the solar source resposible for the ^{3}He-rich SEP in this study. The ^{3}He enrichment might also depend on the occurrence rate of coronal jets and the duration of ejection time seen in our observations.

Acknowledgements. We thank the SDO, WIND/WAVES, ACE and STEREO team for the data. This work was supported by National Science Council of Taiwan under grant NSC 103-2917-I-564-007 and the Postdoctoral Research Abroad Program, and by NASA under grant NNX13AR20G/115828.

References

Archontis, V., Tsinganos, K., & Gontikakis, C. 2010, A&A, 512, L2
Bucik, R., Innes, D. E., Mall, U., Korth, A., & Mason, G. M. 2013, Proc. 33rd ICRC (Rio de Janeiro), paper SH-EX 0552 [arXiv:1307.6342]

Bučík, R., Innes, D. E., Mall, U., et al. 2014, ApJ, 786, 71
Cane, H. V., McGuire, R. E., & von Rosenvinge, T. T. 1986, ApJ, 301, 448
Cane, H. V., Reames, D. V., & von Rosenvinge, T. T. 1988, J. Geophys. Res., 93, 9555
Canfield, R. C., Reardon, K. P., Leka, K. D., et al. 1996, ApJ, 464, 1016
Cliver, E. W., Kahler, S. W., & McIntosh, P. S. 1983, ApJ, 264, 699
Fisk, L. A. 1978, ApJ, 224, 1048
Hsieh, K. C., & Simpson, J. A. 1970, ApJ, 162, L191
Innes, D. E., Cameron, R. H., & Solanki, S. K. 2011, A&A, 531, L13
Kahler, S. W., Sheeley, Jr., N. R., Howard, R. A., et al. 1984, J. Geophys. Res., 89, 9683
Klassen, A., Gómez-Herrero, R., & Heber, B. 2011, Sol. Phys., 273, 413
Klecker, B., Hovestadt, D., Scholer, M., et al. 1984, ApJ, 281, 458
Klecker, B., Möbius, E., & Popecki, M. A. 2007, Space Sci. Rev., 130, 273
Klein, K.-L., & Posner, A. 2005, A&A, 438, 1029
Kocharov, L., Laivola, J., Mason, G. M., Didkovsky, L., & Judge, D. L. 2008, ApJS, 176, 497
Krucker, S., Kontar, E. P., Christe, S., Glesener, L., & Lin, R. P. 2011, ApJ, 742, 82
Kundu, M. R., Raulin, J. P., Nitta, N., et al. 1995, ApJ, 447, L135
Lin, R. P. 1985, Sol. Phys., 100, 537
Luhn, A., Klecker, B., Hovestadt, D., & Moebius, E. 1987, ApJ, 317, 951
Mandrini, C. H., Schmieder, B., Démoulin, P., Guo, Y., & Cristiani, G. D. 2014, Sol. Phys., 289, 2041
Mason, G. M. 2007, ^{3}He-Rich Solar Energetic Particle Events, eds. R. von Steiger, G. Gloeckler, & G. M. Mason (Springer Science+Business Media), 231
Mason, G. M., Reames, D. V., von Rosenvinge, T. T., Klecker, B., & Hovestadt, D. 1986, ApJ, 303, 849
Mason, G. M., Gold, R. E., Krimigis, S. M., et al. 1998, Space Sci. Rev., 86, 409
Mason, G. M., Dwyer, J. R., & Mazur, J. E. 2000, ApJ, 545, L157
Moreno-Insertis, F., Galsgaard, K., & Ugarte-Urra, I. 2008, ApJ, 673, L211
Nitta, N. V., & De Rosa, M. L. 2008, ApJ, 673, L207
Nitta, N. V., Reames, D. V., De Rosa, M. L., et al. 2006, ApJ, 650, 438
Pick, M., Mason, G. M., Wang, Y.-M., Tan, C., & Wang, L. 2006, ApJ, 648, 1247
Reames, D. V. 1999, Space Sci. Rev., 90, 413
Reames, D. V., & Stone, R. G. 1986, ApJ, 308, 902
Reames, D. V., von Rosenvinge, T. T., & Lin, R. P. 1985, ApJ, 292, 716
Reames, D. V., Dennis, B. R., Stone, R. G., & Lin, R. P. 1988, ApJ, 327, 998
Schrijver, C. J., & De Rosa, M. L. 2003, Sol. Phys., 212, 165
Temerin, M., & Roth, I. 1992, ApJ, 391, L105
Wang, Y.-M., Pick, M., & Mason, G. M. 2006, ApJ, 639, 495
Yokoyama, T., & Shibata, K. 1996, PASJ, 48, 353